Role of Coulomb correlations in the charge density wave of CuTe

Sooran Kim,[1] Bongjae Kim,[2,3] and Kyoo Kim[3,4,*]

[1]*Department of Physics Education, Kyungpook National University, Daegu 41566, Korea*
[2]*Department of Physics, Kunsan National University, Gunsan 54150, Korea*
[3]*Max Planck POSTECH/Hsinchu Center for Complex Phase Materials, Pohang University of Science and Technology, Pohang 37673, Korea*
[4]*Department of Physics, Pohang University of Science and Technology, Pohang 37673, Korea*

(Received 28 May 2019; revised manuscript received 18 July 2019; published 26 August 2019)

A quasi-one-dimensional layered material CuTe undergoes a charge density wave (CDW) transition in Te chains with a modulation vector of $q_{\mathrm{CDW}} = (0.4, 0.0, 0.5)$. Despite the clear experimental evidence for the CDW, the theoretical understanding, especially the role of the electron-electron correlation in the CDW, has not been fully explored. Here, using first-principles calculations, we demonstrate that the correlation effect of Cu is critical to stabilize the $5 \times 1 \times 2$ modulation of Te chains. We find that the phonon calculation with the strong Coulomb correlation exhibits the imaginary phonon frequency, i.e., the so-called phonon soft mode, at $q_{ph0} = (0.4, 0.0, 0.5)$, indicating the structural instability. The corresponding lattice distortion of the soft mode agrees well with the experimental modulation. These results demonstrate that the CDW transition in CuTe originates from the interplay of the Coulomb correlation and electron-phonon interaction.

DOI: 10.1103/PhysRevB.100.054112

I. INTRODUCTION

The novel electronic and magnetic properties of low-dimensional materials have drawn interest because of their fundamental physics and possible applications [1–6]. The intrinsic instabilities in low-dimensional systems often trigger a charge density wave (CDW), Peierls transitions, spin density wave, or even unconventional superconductivity [7–11]. Peierls-type transitions are experimentally observed in quasi-one-dimensional (quasi-1D) materials such as tetrathiafulvalene-tetracyanonitrodimethane (TTF-TCNQ) molecular solid *trans*-polyacetylene polymers, MQ_3 (M = Ta, Nb and Q = S, Se) and $K_{0.3}MoO_3$ [12–20] (see Table I in Ref. [15]).

Electronic instability, however, widely understood as the origin of a Peierls transition, has been challenged [10,11,21,22]. As the dimension of interatomic connection increases, the susceptibility peak feature becomes weakened, and other mechanisms such as electron-phonon interaction become important in the realization of a Peierls-type structural or CDW transition. Sometimes the role of the underlying 1D interatomic network can be pronounced due to the directional bonding, for instance, of p orbitals in elements such as Se, Te, and I, resulting in strong 1D Peierls-type structural transitions in higher dimensions [23,24]. Furthermore, even though the Peierls transition does not require the strong electron-electron correlation as in the Mott transition, there have been reports on the role of strong Coulomb correlation in the Peierls transition, dubbed as a Mott-Peierls transition, especially in VO_2 [25–30]. Therefore elucidating the mechanism of CDW transitions, which can originate from the Fermi-surface nesting, electron-phonon interaction, electron-electron correlation, or even the interplay of them, would be interesting and important for fundamental physics in low-dimensional systems.

The crystal CuTe, called vulcanite, is one of the prototypical quasi-1D systems, which undergoes a CDW transition at $T_{\mathrm{CDW}} = 335$ K. The early x-ray diffraction study reported that CuTe is crystallized in the strained FeTe-like orthorhombic unit cell with the space group *Pmmn* (No. 59), which consists of one formula unit of CuTe [31]. As shown in Figs. 1(a) and 1(b), Te atoms form a distorted square planar net resulting in the quasi-1D chain structure, and Cu atoms have a planar square network with buckling in the non-CDW phase of CuTe.

According to the tight-binding calculation of Seong *et al.*, a dimer formation with $q = (0.5, 0.0, 0.0)$ is stabilized over the nondimerized state and opens a band gap, which suggests the possibility of the structural transition accompanying a metal-insulator transition [32]. More recent x-ray diffraction, as well as a high-resolution tunneling electron microscopy experiment, observed a structural modulation of the Te chain with $q_{\mathrm{CDW}} = (0.4, 0.0, 0.5)$, as shown in Fig. 1(c) [33]. The CDW transition in CuTe is also investigated utilizing angle-resolved photoemission spectroscopy (ARPES) and analyzed with first-principles calculations [34]. The momentum-dependent gap opening of 0.1–0.2 eV for a quasi-1D band is clearly observed below T_{CDW} in the ARPES signals. They also demonstrated the band structure evolution with temperature from 20 to 350 K and potassium doping, and the eventual disappearance of the CDW gap feature. Both Fermi-surface nesting and electron-phonon coupling were reported as an origin of the CDW instability from a peak feature in the bare charge susceptibility and a Kohn anomaly in the phonon calculation at q_{CDW}. Their phonon dispersion curve, however, does not show the imaginary phonon frequency at q_{CDW}, which is the evidence of the structural instability [34].

*kyoo@mpk.or.kr

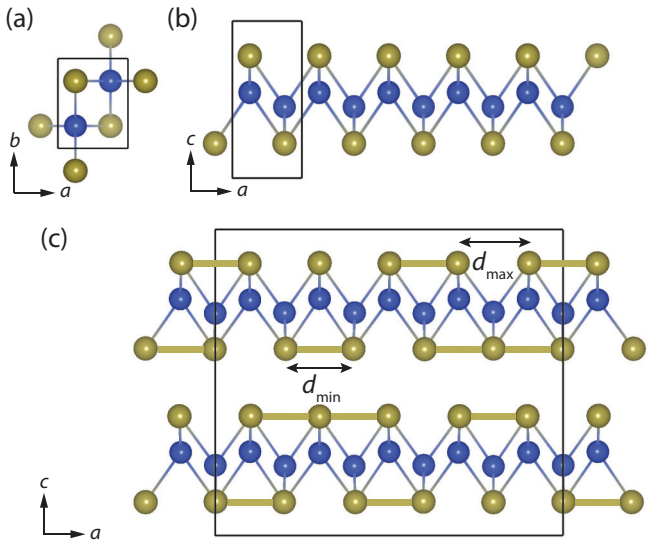

FIG. 1. Crystal structures of CuTe. Blue and yellow balls represent Cu and Te, respectively. High-symmetric structure in the non-CDW phase at a high temperature: (a) top view, (b) side view. (c) $5 \times 1 \times 2$ modulated structure in the CDW phase. The bond between Te atoms illustrates the Te modulation along the a direction reported in Refs. [33,34]. d_{min} and d_{max} indicate the shortest and longest distances among Te-Te bondings, respectively.

To unveil the microscopic mechanism of the CDW transition, in this paper, we present the electronic structure and lattice dynamics of CuTe by first-principles calculations. In particular, we focus on the Coulomb correlation of Cu ion because of its partial occupied d orbitals. We considered various types of van der Waals interaction schemes, exchange-correlation functionals, and electron-electron correlation strength to explore the origin of the modulation. Among them, we find that the strong Coulomb correlation of Cu d orbitals has an essential role in triggering the CDW transition. The phonon dispersion curve with considering the correlation effect provides the imaginary frequency whose corresponding lattice displacement is exactly consistent with the experimental Te modulation.

II. COMPUTATIONAL DETAILS

Density functional theory (DFT) calculations for structural relaxations and force calculations were performed by the Vienna *ab initio* simulation package, VASP [35]. PHONOPY was used for phonon calculations [36]. A full-potential local-orbital minimum-basis code (FPLO) was employed to analyze the detailed band structure including band unfolding [37].

We included the spin-orbit coupling (SOC) and utilized two exchange-correlation functionals: Perdew-Burke-Ernzerhof (PBE) [38] and PBEsol (revised PBE for solid) [39]. We performed the PBE + U calculations to account for the correlated d orbitals of Cu with the Dudarev implementation [40]. $U_{eff} = U - J$ in a range of 2 to 13 eV is tested to investigate the Coulomb correlation effect on the structural instability. Three different types of van der Waals interaction schemes are also checked: DFT-D3 method with zero damping (D3) [41] and Becke-Jonson damping (D3-BJ) [42], and D2 method of Grimme (D2) [43]. The energy cut for the plane waves in the overall calculation is 400 eV. For the structural relaxations, the **k**-point samplings for the non-CDW and the CDW structure are $20 \times 16 \times 8$ and $4 \times 16 \times 4$, respectively.

For the phonon calculation, the dynamical matrix is obtained with the finite displacements method (frozen phonon method) using the $10 \times 1 \times 2$ supercell, based on the Hellmann-Feynman theorem [36,44]. Before carrying out the phonon calculations, we performed the atomic relaxation using experimental lattice parameters [33]. The **k**-point sampling of $3 \times 16 \times 4$ is used for the $10 \times 1 \times 2$ supercell.

To obtain a reasonable range of Coulomb correlation parameters of Cu atoms, we have employed the linear response method [45] implemented in QUANTUM ESPRESSO [46]. The dense $(48 \times 36 \times 24)$ **k** mesh is used for the high-symmetric primitive unit cell. The energy cut for wave functions and the kinetic-energy cut for charge density and potential are 45 and 250 Ry, respectively.

III. RESULTS AND DISCUSSIONS

To investigate the instability of the Te chains, we relaxed the internal parameters of the $5 \times 1 \times 2$ supercell, starting from the experimental one [33], and obtained d_{min} and d_{max} (see Fig. 1) in Te chains in various simulation conditions employing diverse types of van der Waals interactions and functional, varying Coulomb correlation parameters (U_{eff}), and for the hole-doping case. The modulated CDW structure is relaxed back to the high-symmetric non-CDW structure, losing the formation of the Te modulation except when the Coulomb correlation for Cu d orbitals is considered. This result is consistent with the stable phonon dispersion curve of Zhang *et al.* [34], where strong Coulomb correlation is not included.

Figure 2 shows the calculated d_{min} and d_{max} depending on the U_{eff}. As U_{eff} increases, clear bifurcation of d_{min} and d_{max} is observed, and their values are progressively reaching the experimental values regardless of the van der Waals correction.

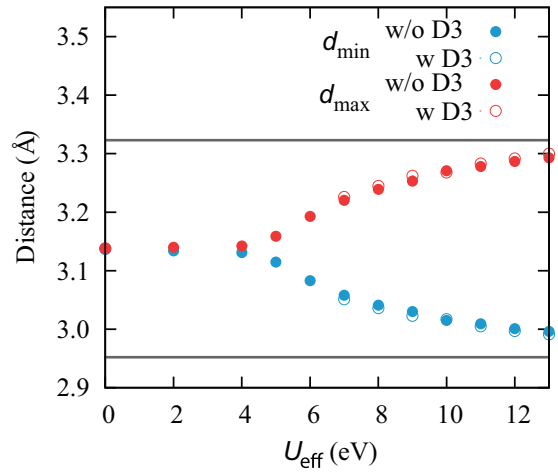

FIG. 2. Distances of the Te-Te bonding as a function of U_{eff}. The solid (black) and dotted (red and blue) lines represent the distances after the relaxation without and with the van der Waals interaction with the D3 method, respectively. The gray lines at the bottom and top indicate the experimental values.

TABLE I. Calculated lattice parameters and atomic positions of the non-CDW phase depending on the simulation condition. U9 means the U_{eff} of 9 eV.

Functional	a	b	c	z_{Cu}	z_{Te}
PBE	3.280	4.018	7.457	0.466	0.242
PBEsol	3.197	3.949	6.921	0.463	0.222
PBE + vdW	3.170	3.996	6.919	0.457	0.219
PBE + D3 + U9	3.081	4.035	6.986	0.455	0.220
PBE + D2 + U9	3.093	4.033	6.947	0.452	0.219
PBE + D3-BJ + U9	3.074	4.010	6.830	0.455	0.214
PBE + U9	3.138	4.101	7.415	0.459	0.236
Expt*	3.138	4.059	6.902	0.454	0.221

When the U_{eff} is larger than 9 eV, the differences between the calculated and the experimental d_{min} and d_{max} are less than 3%. Previous papers have chosen the U value > 6.5 eV for a Cu atom in the copper oxides case [47–51]. Furthermore, to ensure the reliability of our U_{eff} value, we performed the linear response method, which can serve as a guide for the estimation of the U parameter in a self-consistent way. The calculated U_{eff} for Cu atoms is 11.5 eV, which agrees well with our finding in Fig. 2. This relatively large U_{eff} serves as a role for pushing Cu weight to higher binding energy and strengthening the Te character at the Fermi level, as will be discussed later.

In addition, we performed full relaxation using the non-CDW structure as in Figs. 1(a) and 1(b). Adding Coulomb correlation with U_{eff} of 9 eV, lattice parameters a and c slightly decrease while lattice parameter b increases compared to the PBE value. All of a, b, and c lattice parameters further decrease with van der Waals interaction. In particular, the lattice parameter c is reproduced well with the inclusion of the van der Waals interaction and PBEsol functional as in Table I. However, other lattice parameters, a and b, and atomic positions do not considerably depend on the simulation conditions. Also, the scheme dependence of van der Waals correction is not significant. All calculated lattice parameters and atomic positions are comparable to the experimental values regardless of the condition.

The correlation effect of the Cu d orbitals is investigated by observing the band dispersion and density of states (DOS) without [Fig. 3(a)] and with U [Fig. 3(b)]. The band dispersion is dominated by Te p_x (σ bond along the a axis) and p_y (π bond along the a axis) near the Fermi level, and E_f is hardly affected by the inclusion of U. However, the strong Cu weight redistribution to higher binding energy centering, -5 eV, is observed, which suggests a non-negligible modification in Cu-Te hybridization near the E_f. As a result, the Te character becomes more pronounced at the E_f as in Fig. 3(b). The Cu weight shift from Fermi level can strengthen the 1D nature by removing the Cu-Te hopping channel, which is a suitable condition for the CDW transition. Note that Cu bands are located in the range of -2 to -4 eV, and in the range of -4 to -6 eV in PBE and PBE + U calculations, respectively. Thus, the experimental measurement of Cu weight might be interesting to check the correlation effect of Cu. In addition, we performed the PBE + U calculations without SOC. The effect of SOC is not significant, especially for quasi-1D bands,

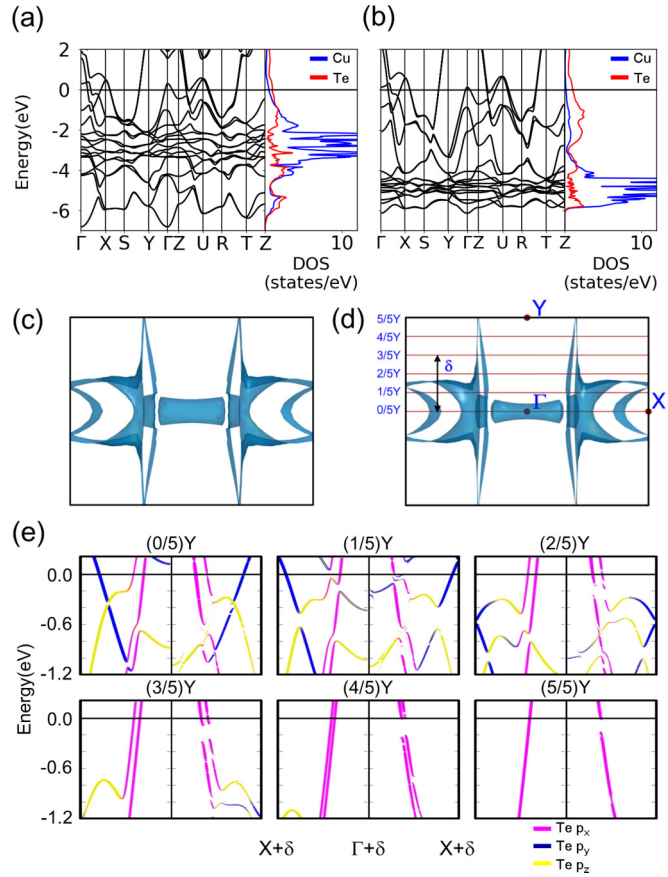

FIG. 3. Band structures and DOS of the non-CDW structure with (a) PBE and (b) PBE + U. Top view of Fermi surface in the X-Γ-Y plane with (c) PBE and (d) PBE + U. (e) Band structures along paths Gamma-X shifted by δ=(0, $\alpha \times 0.5$, 0) with (α= 0, 1/5, 2/5, 3/5, 4/5, and 5/5), which are indicated with red lines in (d). On each figure with a corresponding δ value on top, the band structure of the non-CDW structure (left) is compared to the one of the CDW structure (right) as a mirror image.

implying that the SOC does not play a critical role in the CDW transition.

The Fermi surfaces (FSs) of the non-CDW structure within PBE and PBE + U are compared as shown in Figs. 3(c) and 3(d), respectively. The quasi-1D-like FS, which is parallel to the Γ-Y path, comes from Te 1D chain. This FS becomes more flattened with the inclusion of U, as in Fig. 3(d), implying the enhanced nesting feature. As the CDW occurs, a partial gap opens in this quasi-1D band. Figure 3(e) shows the modification of band structures with the Te modulation: six figures present the unfolded band structure along Γ-X shifted by $\delta = \alpha$Y ($\alpha = 0$, 1/5, 2/5, 3/5, 4/5, and 5/5), indicated as red guidelines in Fig. 3(d). The most announced change occurs in the Te p_x channel as expected. The band gap starts to open when $\alpha > 2/5$, which is consistent with the gap size dispersion along k_y in the previous experiment [34]. The overall feature of Te weight agrees well with the experimental observation of the CDW band gap formed by Te p_x orbitals. In addition, our data and previous unfolding data [34] require a slight shift in energy to match with the experimental results. This need for the shift of the Fermi level naturally raised the question of whether hole doping alone can be the origin of the

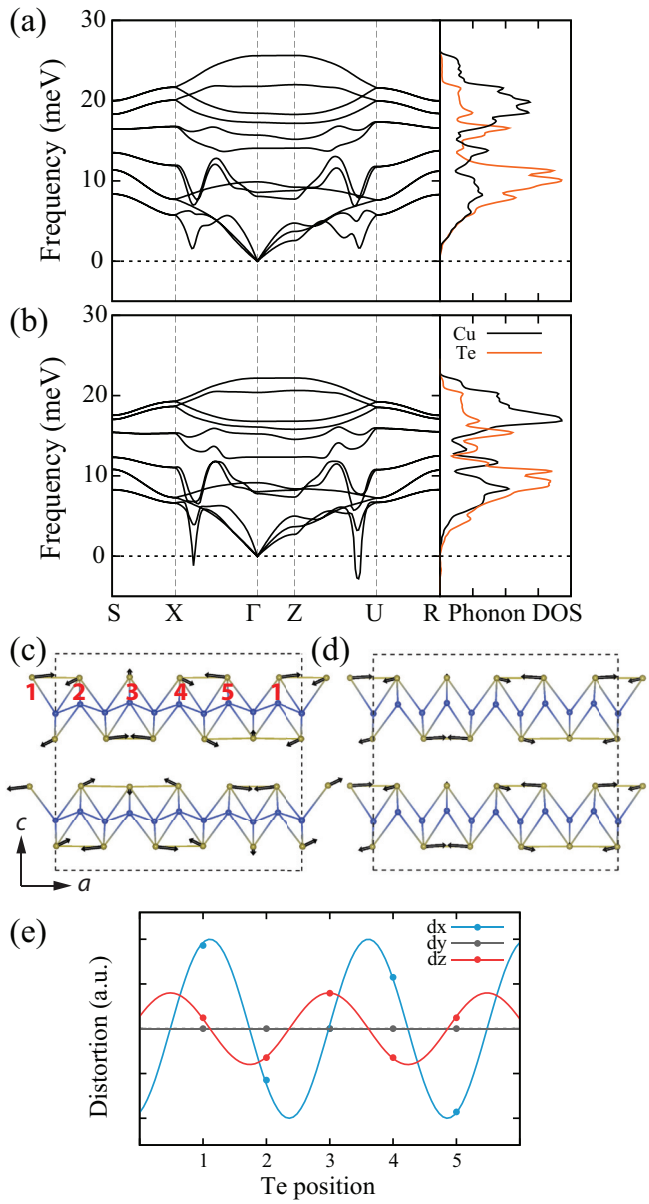

FIG. 4. Phonon dispersion curves and phonon DOSs of CuTe: (a) result from the PBE and (b) result from the PBE + U. The imaginary phonon frequencies imply the structural instability. Lattice displacements by the phonon soft modes at (c) $q_{ph0} = (0.4, 0.0, 0.5)$ and (d) $q_{ph1} = (0.4, 0.0, 0.0)$. (e) Te distortions ($dx$, dy, dz) by the phonon soft mode at q_{ph0}. Each Te position is indicated by the number in red in (c). Data are fitted with sine functions as a guide.

CDW transition. Accordingly, we relaxed the CDW structure without Coulomb correlation with hole doping, by removing electrons while keeping charge neutrality with background charge. However, the non-CDW structure is restored, which suggests that the doping-derived CDW transition scenario is not likely.

Figures 4(a) and 4(b) show the phonon dispersion curves of the non-CDW state using PBE and PBE + U, respectively. We did not include the SOC for the PBE case to compare with previous phonon calculations [34,52]. The phonon structures of PBE + U without SOC and PBE + U + D3 are qualitatively the same with that of PBE + U in Fig. 4(b), which show the imaginary phonon frequencies at $q_{ph0} = (0.4, 0.0, 0.5)$ and at $q_{ph1} = (0.4, 0.0, 0.0)$. The imaginary phonon frequency, i.e., the so-called phonon soft mode, indicates the structural instability. This demonstrates the critical role of the Coulomb correlation of Cu d electrons in the CDW, which is consistent with the structure relaxation results shown above. The phonon bands soften with the addition of the Coulomb correlation. In particular, as in the phonon DOSs of Fig. 4, while the Te and Cu phonon bands in the PBE result are similarly occupied at a low-frequency range below 5 meV, the Te bands are more occupied and Cu bands are less occupied at the low-frequency range in the PBE + U calculation. The phonon DOSs show that with inclusion of U, Cu weight becomes decoupled in the low-frequency region where the soft mode is located, which supports our weakened Cu-Te bonding scenario from the electronic DOS analysis. It is worth noting that the correlation of Cu d adjusts not only Cu phonon bands but also Te phonon bands, leading to the imaginary phonon frequency of the Te phonon bands. The non-CDW structure exhibits a stable phonon dispersion curve in Fig. 4(a) (also reported by Zhang *et al.* [34]) without consideration of the Coulomb correlation despite the experimentally unstable non-CDW structure at a low temperature. The correlation-assisted phonon soft mode and structural transition, as in Fig. 4(b), has been reported in similar quasi-1D systems [29,30].

The phonon instability at q_{ph0} reproduces the the experimental q_{CDW}. Figures 4(c) and 4(d) illustrate the lattice displacements of the softened phonon mode at q_{ph0} and q_{ph1}, respectively. This displacement of Te atoms at q_{ph0} generates $5 \times 1 \times 2$ modulation of Te chains, which are not captured in the previous phonon calculations [34,52]. Figure 4(e) shows the distortions (dx, dy, dz) of each Te atom indicated by numbers in Fig. 4(c). The distortions of each Te along the a (dx) and c (dz) directions are sinusoidal with the periodicity of $0.4 \times 2\pi$. The amplitude of dx is larger than that of dz. The amplitude of dy is equaled to 0, which means no modulation along the b direction. These features agree well with the experiment in Ref. [33]. The distortions of the different Te layers are reproduced by a phase shift. Our results demonstrate that the electron-electron correlation and electron-phonon coupling play an essential role in driving the CDW. In addition, the corresponding lattice displacement of the phonon soft mode at q_{ph1} also contains the same Te-Te modulation in a layer, but does not change along the c direction. The relaxed structure from q_{ph0} modulation has lower energy of 1.6 meV than that from q_{ph1} modulation. It explains why the CDW occurs at q_{ph0} but not at q_{ph1}. The phonon instability is mostly related to the Te quasi-1D chain. And the small energy difference between q_{ph0} and q_{ph1} is related to chain-chain interaction which is the second-order effect.

IV. CONCLUSIONS

In conclusion, we demonstrated, using DFT and phonon analysis, that the Coulomb correlation of the Cu $3d$ orbital plays an indirect but crucial role in the CDW transition of Te chains in the layered CuTe. We found that the inclusion of U pushes away Cu d orbitals from E_f to the higher

binding energy region and, accordingly, weakens the Cu-Te bonding. This strengthens the 1D nature of Te-Te bonding in the Te chain, resulting in the CDW instability. Only with the inclusion of the Coulomb correlation in Cu atom do we observed the experimentally consistent imaginary phonon soft mode whose corresponding lattice distortion reproduces the CDW modulation. We believe that our work can shed light on the understanding of a mechanism of CDW transitions, especially when the interplay of multiple physical parameters is in effect.

ACKNOWLEDGMENTS

We acknowledge the fruitful discussion with J. H. Shim and K.-T. Ko. This work was supported by the NRF Grant (Contracts No. 2016R1D1A1B02008461, No. 2018R1D1A1A02086051, and No. 2019R1F1A1052026), Max-Plank POSTECH/KOREA Research Initiative (Grant No. 2016K1A4A4A01922028), and the KISTI supercomputing center (Projects No. KSC-2018-CRE-0075 and No. KSC-2018-CRE-0079).

[1] H. L. Stormer, Rev. Mod. Phys. **71**, 875 (1998).
[2] C. Zeng, P. R. C. Kent, T.-H. Kim, A.-P. LI, and H. H. Weitering, Nat. Mater. **7**, 539 (2008).
[3] K. S. Burch, D. Mandrus, and J.-G. Park, Nature (London) **563**, 47 (2018).
[4] K. Kim, J. Seo, E. Lee, K.-T. Ko, B. S. Kim, B. G. Jang, J. M. Ok, J. Lee, Y. J. Jo, W. Kang, J. H. Shim, C. Kim, H. W. Yeom, B. I. Min, B.-J. Yang, and J. S. Kim, Nat. Mater. **17**, 794 (2018).
[5] M. Gibertini, M. Koperski, A. F. Morpurgo, and K. S. Novoselov, Nat. Nanotechnol. **14**, 408 (2019).
[6] X. Chia and M. Pumera, Nat. Catal. **1**, 909 (2018).
[7] P. A. Lee, N. Nagaosa, and X.-G. Wen, Rev. Mod. Phys. **78**, 17 (2006).
[8] Y. Cao, V. Fatemi, S. Fang, K. Watanabe, T. Taniguchi, E. Kaxiras, and P. Jarillo-Herrero, Nature (London) **556**, 43 (2018).
[9] A. M. Gabovich. A. I. Voitenko, J. F. Annett, and M. Ausloos, Supercond. Sci. Technol. **14**, R1 (2001).
[10] X. Zhu, Y. Cao, J. Zhang, E. W. Plummer, and J. Gui, Proc. Natl. Acad. Sci. USA **112**, 2367 (2015).
[11] X. Zhu, J. Guo, J. Zhang, and E. W. Plummer, Adv. Phys. X **2**, 622 (2017).
[12] F. Denoyer, R. Comès, A. F. Garito, and A. J. Heeger, Phys. Rev. Lett. **35**, 445 (1975).
[13] D. Jérome, Chem. Rev. **104**, 5565 (2004).
[14] S. Kagoshima, H. Anzai, K. Kajimura, and T. Ishiguro, J. Phys. Soc. Jpn. **39**, 1143 (1975).
[15] S. van Smaalen, Acta Cryst. A **61**, 51 (2005).
[16] T. Sambongi, K. Tsutsumi, Y. Shiozaki, M. Yamamoto, K. Yamaya, and Y. Abe, Solid State Commun. **22**, 729 (1977).
[17] Z. Z. Wang, P. Monceau, H. Salva, C. Roucau, L. Guemas, and A. Meerschaut, Phys. Rev. B **40**, 11589 (1989).
[18] F. W. Boswell and A. Prodan, Physica B+C **99**, 361 (1980).
[19] J. P. Pouget, C. Noguera, A. H. Moudden, and R. Moret, J. Phys. (France) **46**, 1731 (1985).
[20] R. M. Fleming, L. F. Schneemeyer, and D. E. Moncton, Phys. Rev. B **31**, 899 (1985).
[21] M. D. Johannes and I. I. Mazin, Phys. Rev. B **77**, 165135 (2008).
[22] D. Kartoon, U. Argaman, and G. Makov, Phys. Rev. B **98**, 165429 (2018).
[23] A. Decker, G. A. Landrum, and R. Dronskowski, Z. Anorg. Allg. Chem. **628**, 295 (2002).
[24] B. I. Min, J. H. Shim, M. S. Park, K. Kim, S. K. Kwon, and S. J. Youn, Phys. Rev. B **73**, 132102 (2006).
[25] E. Jeckelmann, Phys. Rev. B **57**, 11838 (1998).
[26] P. Sengupta, A. W. Sandvik, and D. K. Campbell, Phys. Rev. B **67**, 245103 (2003).
[27] S. Biermann, A. Poteryaev, A. I. Lichtenstein, and A. Georges, Phys. Rev. Lett. **94**, 026404 (2005).
[28] M. W. Haverkort, Z. Hu, A. Tanaka, W. Reichelt, S. V. Streltsov, M. A. Korotin, V. I. Anisimov, H. H. Hsieh, H.-J. Lin, C. T. Chen, D. I. Khomskii, and L. H. Tjeng, Phys. Rev. Lett. **95**, 196404 (2005).
[29] S. Kim, K. Kim, C.-J. Kang, and B. I. Min, Phys. Rev. B **87**, 195106 (2013).
[30] S. Kim, K. Kim, and B. I. Min, Phys. Rev. B **90**, 045124 (2014).
[31] F. Pertlik, Mineal. Petrol. **71**, 149 (2001).
[32] S. Seong, T. A. Albright, X. Zhang, and M. Kanatzidis, J. Am. Chem. Soc. **116**, 7287 (1994).
[33] K. Stolze, A. Isaeva, F. Nitsche, U. Burkhardt, H. Lichte, D. Wolf, and T. Doert, Angew. Chem Int. Ed. **52**, 862 (2013).
[34] K. Zhang, X. Liu, H. Zhang, K. Deng, M. Yan, W. Yao, M. Zheng, E. F. Schwier, K. Shimada, J. D. Denlinger, Y. Wu, W. Duan, and S. Zhou, Phys. Rev. Lett. **121**, 206402 (2018).
[35] G. Kresse and J. Furthmüller, Phys. Rev. B **54**, 11169 (1996); Comput. Mater. Sci. **6**, 15 (1996).
[36] A. Togo, F. Oba, and I. Tanaka, Phys. Rev. B **78**, 134106 (2008).
[37] W. Ku, T. Berlijn, and C.-C. Lee, Phys. Rev. Lett. **104**, 216401 (2010).
[38] J. P. Perdew, K. Burke, and M. Ernzerhof, Phys. Rev. Lett. **77**, 3865 (1996).
[39] J. P. Perdew, A. Ruzsinszky, G. I. Csonka, O. A. Vydrov, G. E. Scuseria, L. A. Constantin, X. Zhou, and K. Burke, Phys. Rev. Lett. **100**, 136406 (2008).
[40] S. L. Dudarev, G. A. Botton, S. Y. Savrasov, C. J. Humphreys, and A. P. Sutton, Phys. Rev. B **57**, 1505 (1998).
[41] S. Grimme, J. Antony, S. Ehrlich, and S. Krieg, J. Chem. Phys. **132**, 154104 (2010).
[42] S. Grimme, S. Ehrlich, and L. Goerigk, J. Comput. Chem. **32**, 1456 (2011).
[43] S. Grimme, J. Comput. Chem. **27**, 1787 (2006).
[44] K. Parlinski, Z. Q. Li, and Y. Kawazoe, Phys. Rev. Lett. **78**, 4063 (1997).
[45] M. Cococcioni and S. de Gironcoli, Phys. Rev. B **71**, 035105 (2005).
[46] P. Giannozzi, S. Baroni, N. Bonini, M. Calandra, R. Car, C. Cavazzoni, D. Ceresoli, G. L. Chiarotti, M. Cococcioni, I. Dabo, A. Dal Corso, S. Fabris, G. Fratesi, S. de Gironcoli, R. Gebauer, U. Gerstmann, C. Gougoussis, A. Kokalj, M. Lazzeri,

L. Martin-Samos, N. Marzari, F. Mauri, R. Mazzarello, S. Paolini, A. Pasquarello, L. Paulatto, C. Sbraccia, S. Scandolo, G. Sclauzero, A. P. Seitsonen, A. Smogunov, P. Umari, and R. M. Wentzcovitch, J. Phys.: Condens. Matter **21**, 395502 (2009).

[47] V. I. Anisimov, J. Zaanen, and O. K. Andersen, Phys. Rev. B **44**, 943 (1991).

[48] C. E. Ekuma, V. I. Anisimov, J. Moreno, and M. Jarrell, Eur. Phys. J. B **87**, 23 (2014).

[49] M. Nolan and S. D. Elliott, Phys. Chem. Chem. Phys. **8**, 5350 (2006).

[50] I. S. Elfimov, G. A. Sawatzky, and A. Damascelli, Phys. Rev. B **77**, 060504(R) (2008).

[51] A. K. Mishra, A. Roldan, and N. H. de Leeuw, J. Phys. Chem. C **120**, 2198 (2016).

[52] J. U. Salmón-Gamboa, A. H. Barajas-Aguilar, L. I. Ruiz-Ortega, A. M. Garay-Tapia, and S. J. Jiménez-Sandoval, Sci. Rep. **8**, 8093 (2018).